https://doi.org/10.5194/egusphere-2022-126
Preprint. Discussion started: 30 May 2022

Responses of CIPS/AIM Noctilucent Clouds to the Interplanetary Magnetic Field

Liang Zhang[1], Brian Tinsley[2], Limin Zhou[3,4]

[1]State Key Laboratory of Marine Geology, Tongji University, Shanghai, 200092, China
[2]Physics Department, University of Texas at Dallas, Richardson, Texas, 75080, USA
[3]Key Laboratory of Geographic Information Science, East China Normal University, Shanghai, 200062, China
[4]State Key Laboratory of Numerical Modeling for Atmospheric Sciences and Geophysical Fluid Dynamics, Beijing, 100029, China

Correspondence to: Liang Zhang (Liangzhang420@tongji.edu.cn)

Abstract. This study investigates the link between the interplanetary magnetic field (IMF) B_y component and the Noctilucent clouds (NLCs) measured by the Cloud Imaging and Particle Size (CIPS) experiment onboard the Aeronomy of ICE in the Mesosphere (AIM) satellite. The mean ice particle radius in NLCs is found to be positively/negatively correlated with *IMF* B_y in the Southern/Northern Hemisphere (SH/NH), respectively, on a day-to-day time scale in most of the 20-summer seasons during the 2007-2017 period with a near 0-day lag time, and the response in the SH is stronger than that in the NH. Moreover, the albedo, ice water content, and frequency of occurrence of NLCs present positive correlation with *IMF* B_y in SH but no significant correlation in NH. The superposed epoch analysis (SEA) further indicates the r_m on average changes by about 0.73 nm after *IMF* B_y reversals, which is significant at 90% confidence level in Monte Carlo sensitivity tests. Our results suggest an *IMF* B_y-driven pathway: the influence of the solar wind on the polar ionospheric electric potential affects the microphysical processes in NLCs, and consequently the ice particle radius and NLC brightness.

1 Introduction

1.1 NLCs

Noctilucent clouds are the highest and coldest clouds in the terrestrial atmosphere, forming in the high latitude summer mesosphere at ~83 km altitude, where the temperature can drop to ~140 K. The long-term trends in NLCs are supposed to be associated with global climate change, while NLCs are not only susceptible to perturbations from lower atmospheric activities such as gravity waves (Gao et al., 2018) and planetary waves (France et al., 2018), but may also be affected by solar activities on various time scales, including solar proton events (Bardeen et al., 2016; Winkler et al., 2012), the 27-day solar rotation (Robert et al., 2010; Thomas et al., 2015; Thurairajah et al., 2017), and the 11-year solar cycle (Dalin et al., 2018; DeLand and Thomas, 2019; Hervig et al., 2019). To distinguish the contribution of solar activity to polar mesospheric clouds from that of climate change, it is important to clarify the mechanisms of the solar influence on NLCs. Based on the

https://doi.org/10.5194/egusphere-2022-126
Preprint. Discussion started: 30 May 2022

observed modest anti-correlation in NLCs with the 27-day and 11-year solar variations, both photodissociation and dynamic origins have been proposed in which the solar ultraviolet irradiance as characterized by the Lyman alpha (*Ly-α*) index is supposed to play a key role by altering the water vapor and temperature of NLCs (Dalin et al., 2018; Thomas et al., 2015), while in general the exact mechanism is still unclear. In this paper, the *IMF* B_y rather than the *Ly-α* is applied as the solar activity index to explore the solar wind-NLC link, and a new hypotheses will be discussed in the next section.

1.2 *IMF* B_y-related mechanisms for NLC-Solar link

The main *IMF* B_y-related process is the change of ionospheric potential in polar cap regions, which determines the flow of the regional downward ionosphere-earth current density J_Z. The current flow is part of the global atmospheric electric circuit (GEC), with ionospheric potential being ~250 kV positive relative to Earth's surface, maintained by the global thunderstorms and electrified clouds (Slyunyaev et al., 2019; Williams and Mareev, 2014). The Earth experiences a Lorentz electric field applied by the cross product of solar wind magnetic field and velocity, which is mainly northward/southward for positive/negative (duskward/dawnward) *IMF* B_y, and observations have shown that the *IMF* B_y-dependent daily-averaged perturbation of ionospheric potential ranges from -30 to 30 kV at high geomagnetic latitudes and is opposite in the SH/NH (Tinsley and Heelis, 1993).

A possible link may exist between the solar wind B_y variations and polar surface meteorology through the ionospheric potential, which has been supported by a variety of observations, in term of polar surface pressure (Lam et al., 2013), geopotential height (Lam et al., 2014), temperature (Freeman and Lam, 2019; Lam et al., 2018), and below-cloud irradiance (Frederick et al., 2019; Frederick and Tinsley, 2018; Tinsley et al., 2021). It should be noted that these observations are characterized by two features: the responses in SH and NH are opposite, in line with the opposite *IMF* B_y-induced ionospheric potential in SH and NH; the delay time is short, lasting only a few days or less. A hypothesis has been proposed to explain the above observations: firstly, solar wind B_y induces changes in the ionospheric electric potential, as well as the downward current density J_Z in the GEC; second, the microphysical processes inside clouds are sufficiently sensitive to space charge generated by J_Z so that the cloud properties such as infrared opacity and albedo will consequently be affected. Finally, polar surface meteorology will be influenced by cloud radiative forcing (Lam and Tinsley, 2016). The invoked cloud microphysical changes have been detailed for individual aerosol-droplet collisions (Zhang et al., 2018, 2019; Zhang and Tinsley, 2017, 2018), but direct measurements in clouds and modelling are required to test this hypothesis.

In comparison with the tropospheric clouds within which many factors are involved, the polar mesospheric clouds provide a relatively pure scenario to study the role played by electric charges in the microphysical process of clouds. By extending the above 'solar - GEC - cloud microphysics - tropospheric meteorology' hypothesis, it is straightforward to propose the '*IMF* B_y - Ionospheric potential - NLC Microphysics - NLC brightness' hypothesis for the polar mesospheric clouds: *IMF* B_y induces changes in polar ionospheric potential, which will then affect electric charges on the ice particles in NLCs with implications for the ice particle formation and growth process, and ultimately affect the macroscopic properties of NLCs.

https://doi.org/10.5194/egusphere-2022-126
Preprint. Discussion started: 30 May 2022

The CIPS/AIM began observing the NLCs in 2007 and 20-summer-season data in SH and NH from 2007 to 2017 are available now. Therefore, we investigated the hypothetical *IMF* B_y-driven solar-NLC link in this study. The paper is structured as follows: Section 2 provides a brief description of the CIPS data and solar wind data. Section 3 presents the results of NLC correlation with *IMF* B_y during the 20 NLC seasons on the day-to-day scale, as well as the superposed epoch analysis for NLCs response to *IMF* B_y reversals. Section 4 discusses the results and Section 5 summarizes our main conclusions.

2 Data

2.1 CIPS/AIM data

The aeronomy of ICE in the Mesosphere (AIM) satellite was launched on 25 April 2007 to a sun-synchronous polar orbit whose local time is mainly midday-midnight at high latitude regions. The Cloud Imaging and Particle Size (CIPS) experiment onboard AIM comprises a panoramic UV nadir imager, consisting of four cameras operating at 265 nm, with a field of view of 120°×80° and a horizontal spatial resolution of 5×5 km. This platform observes the scattered radiance from NLCs, and images the NLCs of ~40°-85° latitude zone for the summer hemisphere ~15 times per day. The CIPS has provided NLC data from the 2007 summer season until now, in terms of ice particle radius, albedo, and IWC, and detailed descriptions of the CIPS data products, calibration, retrieval algorithms, and retrieval uncertainties have been published (Carstens et al., 2013; Lumpe et al., 2013). The CIPS level 2 orbit data provide rectangular images of NLC properties for each of the 15 orbit strips per day, in which a single pixel represents a 25 km2 (5×5 km) area anywhere on the globe and a 5800×1000 km strip region is covered, thus the cloud cover as well as the frequency of occurrence (*FO*) of NLCs can be obtained by counting the number of pixels showing them in the images. This study applied the version 5.20 CIPS polar mesospheric cloud level 2 data to investigate the response of NLCs to solar variations during 10 NLC seasons (from 2007 to 2016) in NH and 10 NLC seasons (from 2007/2008 to 2016/2017) in SH.

2.2 Solar wind data

The solar wind B_y data in GSM format were downloaded online from the GSFC/ SPDF OMNI Web interface (https://omniweb.gsfc.nasa.gov/form/dx1.html). In the geocentric solar magnetospheric (GSM) coordinate system, the origin locates at the center of the Earth, *X* points towards the sun, *Z* lies in the plane of the *X* and geomagnetic dipole and is perpendicular to *X* (roughly northward), *Y* completes the righthanded coordinate system, stretching toward the dusk. The solar wind structures are fairly complex, varying from 2-sector to 4-sector and sometimes irregularly, therefore, during a 27-day solar rotation period, the *IMF* B_y can reverse 2 or 4 or more times, unlike other solar indexes such as *Ly-α* or F10.7 which show regular 27-day period. In order to apply the widely used SEA method, the key days of B_y reversals are listed in Table 1, which have been selected to ensure that during the 5-day period before and after the key day there is no NLCs data missed and that the direction of *IMF* B_y is relatively stable. The *IMF* B_y changing from positive to negative (from negative to

https://doi.org/10.5194/egusphere-2022-126
Preprint. Discussion started: 30 May 2022

positive) is denoted by *p2n* (*n2p*); four groups of dates during 2007 and 2017 are listed in Table 1, corresponding to the *n2p* (28 cases) and *p2n* (29 cases) reversals during NH summer, and the *n2p* (23 cases) and *p2n* (18 cases) reversals during SH summer, respectively.

3 Results

3.1 Correlation analysis of day-to-day responses of NLCs to *IMF* B_y

Figure 1 shows the variations of the daily-averaged solar wind magnetic field and NLC properties during the NLC seasons from 2007 through 2017. The daily-averaged *IMF* B_y varies between -5 nT and 5 nT, as shown in Fig. 1(a-b), and the periods of *IMF* B_y variations are complex, as noted above. Fig. 1(c-h) show the intensity of NLCs in terms of mean ice particle radius (r_m), mean albedo (Alb_m), and mean ice water content (IWC_m), while Fig. 1(i-j) shows the cloud cover of NLCs, as calculated by counting of pixels, and is linearly proportional to *FO*. In order to diminish noise, the NLC data in the latitude bands 65°-85° are used because the NLCs are rarely observed by CIPS below 65° latitude, and an albedo threshold of 5×10^{-6} sr^{-1} was applied. The intensity and coverage of NLC peak ~20 days after the solstice, and show strong seasonal variations, with the exception of the mean ice particle radius, r_m.

Figure 2 shows the correlation coefficients of NLC intensity and coverage anomaly in the 65°-85° latitude zone with *IMF* B_y for each of the 20 summertime seasons, from 2007 to 2016 in the NH and from 2007/2008 to 2016/2017 in the SH. To remove the seasonal variation, the solar signals are extracted by subtracting the 40-day smoothed CIPS data. To avoid the no-cloud days, only the CIPS data during the period of 10 days before and 50 days after the solstice day are used (Fig. 1). The link between the anomalous mean ice particle radius r_m with *IMF* B_y is conspicuous, with positive correlation coefficients in all of the SH summer seasons and negative correlations in most of the NH summer seasons (Fig. 2a). These opposite responses in the SH and NH are consistent with the opposite ionospheric potential changes in SH and NH caused by *IMF* B_y. Further, the response was stronger in the SH, with the correlation coefficient being about twice of that in NH. In NLCs, the larger the ice particle size is, the greater the albedo and IWC are, namely, the mean ice particle radius is normally positively correlated with the albedo and IWC, the 20-seasonal CIPS data show a correlation coefficient of ~0.52 between r_m and Alb_m and of ~0.35 for rm and IWC_m. Conversely, the cloud cover of NLCs will also change in pace with the formation and growth process of ice particle radius, and the 20-seasonal CIPS data also show a correlation coefficient of ~0.48 between r_m and *FO*. It is thus reasonable to speculate that the albedo, IWC, and *FO* will respond to *IMF* B_y in concert with ice particle radius, and Fig. 2(b-d) show the correlation coefficients between the anomaly of Alb_m, IWC_m, and *FO* with *IMF* B_y are pronounced in SH, but not in NH.

Furthermore, Figure 3 shows the mean correlation coefficients for time lags varying from 0 to 6 days. The error bars illustrate the standard deviation of the mean, which are calculated from the 10 seasonal correlation coefficients and are also given in Fig. 2 at 0-day lag time. A very short delay time was observed (Fig. 3), with the maximum correlations occurring near zero day, implying a microphysical response in NLCs to *IMF* B_y similar to the short delay time that has also been

https://doi.org/10.5194/egusphere-2022-126
Preprint. Discussion started: 30 May 2022

observed in the solar-troposphere studies. In previous studies of the link between *Ly-α* and NLCs, the proposed mechanisms involving photodissociation, heating, or circulation all required longer time. In contrast, the *IMF* B_y-related processes of ionospheric potential changes respond quickly to solar wind magnetic field reversals. In summary, the short delay time of NLC properties responding to *IMF* B_y variations implies a mechanism of electro-dynamic origin rather than thermal-dynamic origin.

In order to further verify the response of NLCs to solar wind at different latitudes, the approaches in Fig. 2 were repeated for the five latitude bands of 80°-85°, 75°-80°, 70°-75°, 65°-70°, 60°-65°, respectively. The correlation coefficients of the anomaly of NLC properties with *IMF* B_y are shown in Figure 4, and the slope of the anomaly of NLC properties to *IMF* B_y are given in Figure 5. Fig. 4(a) and 5(a) show that in SH, the correlation and sensitivity of ice particle radius r_m to *IMF* B_y are both greater at higher latitudes, in agreement with the ionospheric potential perturbations caused by *IMF* B_y changes, while in NH the correlation and sensitivity are just about half of that in SH but still significant in latitude higher than 65°. For the 60°-65° latitude region, the results are not significant, this may because at lower latitudes the *IMF* B_y-induced processes are too weak and because the rare NLC occurrences at lower latitudes entail weaker signal/noise. Fig. 4(b-d) and 5(b-d) show that the responses of the anomaly of Alb_m, IWC_m, and *FO* to *IMF* B_y are noticeable for high latitude in SH, and obvious for Alb_m only at latitudes higher than 75° in NH, but are not obvious for IWC_m and *FO* in NH. Dividing the slope given in Fig. 5 by the yearly averaged NLC properties in 65°-85° latitudes bands, then the relative slope can be obtained: (0.71±0.16)%/nT in SH and (-0.28±0.08)%/nT in NH for r_m, (1.36±0.59)%/nT in SH and (-0.52±0.32)%/nT in NH for Alb_m, (0.74±0.48)%/nT in SH and (-0.26±0.28)%/nT in NH for IWC_m, (2.28±1.73)%/nT in SH and (-0.38±0.60)%/nT in NH for *FO*, and in consideration of the ~5 nT amplitude of *IMF* B_y variation during solar wind reversals, the responses of NLC intensity and coverage to *IMF* B_y are not negligible.

In addition, other solar wind parameters such as *IMF* B_z, A_p index and *Ly-α* irradiance have also been examined by the same processes; however, no correlations were found for them at 0-day lag time. The solar wind magnetic field line has an Archimedes spiral pattern, i.e., *IMF* B_x is negatively proportional to *IMF* B_y and a correlation coefficient of about -0.67 between them was obtained during the period of 2007 to 2017, thus similar correlations also exist between *IMF* B_x and NLC properties, but with the opposite sign. The *IMF* B_z corresponds to a dawn-dusk solar wind electric field, and thus can generate a dawn-dusk ionospheric potential drop for both hemispheres, while the sun-synchronous orbit of AIM is designed to be midday-midnight with rare opportunity to pass the dawn-dusk regions, thus the zero correlations observed for NLCs with *IMF* B_z are just as expected.

3.2 Superposed epochs for NLCs response to *IMF* B_y reversals

The superposed epoch analysis is frequently applied in the studies of atmospheric responses to short-term solar variations, in which solar signals are more obvious and easier to be extracted than for decadal or longer-term variations. Although the NLCs only occur in summer, during the 20-season period of CIPS data enough *IMF* B_y reversal cases have been accumulated,

https://doi.org/10.5194/egusphere-2022-126
Preprint. Discussion started: 30 May 2022

as listed in Table 1, allowing the SEA method to be used to explore the NLCs responses. In the SEA method, the ice particle radius distribution is denoted by $f(r)$, where the distribution is of the values of r over the array of pixels on a given day. The averages of $f(r)$ during 3 days before and 3 days after the key day are denoted by $f_{3\text{-}pre}$ and $f_{3\text{-}aft}$ respectively, then the changes of ice particle radius distribution δf during *IMF* B_y reversals are given by $\delta f = f_{3\text{-}aft} - f_{3\text{-}pre}$. The results of δf for the *n2p* and *p2n IMF* B_y reversals in SH given in Table 1 are illustrated in Figure 6, with an albedo threshold of 5×10^{-6} sr^{-1}. The mean ice particle radius r_m can be calculated by integrating the product of radius and its distribution, $r_m=\sum rf(r)$, thus the changes of rm during *IMF* B_y reversals are obtained by $\delta r_m = r_{m,3\_aft} - r_{m,3\_pre} = \sum r\delta f$, and the values of δr_m are given in each panel of Fig. 6. For *n2p/p2n IMF* B_y reversals, the polar ionospheric electric potential will increase/decrease in the SH, and the r_m increases/decreases by about 0.88/1.07 nm in SH as shown in Fig.6. Similarly, the results of NH are illustrated in Figure 7, for *n2p/p2n IMF* B_y reversals, the polar ionospheric electric potential will decrease/increase in the NH, the r_m decreases/increases by about 0.25/0.71 nm in NH as shown in Fig.7. Generally, the ice particle average radius changes by about 0.73 nm during *IMF* B_y reversals, and the responses in SH is stronger than that in NH. The results in Fig. 6-7 were subject to Monte Carlo sensitive tests, in which the same number of key days in Table 1 were randomly generated and δr_m can be calculated by SEA, by repeating this process for one thousand times, the distribution of δr_m are obtained, showing the results in Fig. 6-7 are significant at 90% confidence level.

In addition, we also investigate the responses of NLCs to *IMF* B_y reversals for different brightness of noctilucent clouds, namely, by setting the albedo of NLCs varying by 5×10^{-6} sr^{-1}, the changes of particle radius δr_m for different albedos can be obtained. Figure 8 shows that for NLCs albedo varying from 5×10^{-6} sr^{-1} to 30×10^{-6} sr^{-1}, the particle radius r_m will changes consistently to *IMF* B_y reversals. The results in Fig. 8 further verify that the dark and light NLCs are all sensitive to *IMF* B_y reversals. The results in Fig. 8 also support that the responses of NLCs to *IMF* B_y is stronger in SH than that in NH.

4 Discussion

Our results support the existence of a link between NLCs and solar wind magnetic fields, characterized by the two features of opposite responses in SH and NH in conjunction with a short lag time of 1-day at most, similar to the previously introduced solar-troposphere link.

The 'IMF By - ionospheric potential - NLCs microphysics – NLCs brightness' hypothesis is applied to explain the *IMF* B_y-driven solar-NLCs link: *IMF* B_y will firstly change the ionospheric potential at polar regions, then charge the ice particles inside NLCs and play a role in the ice particle formation or growth process, finally the ice particle radius as well as albedo and IWC will be affected. It's critical to know how the microphysics in NLCs are influenced by the ice particles' charges in this hypothesis, there are two alternatives: one explanation is the agglomeration of ice and dust particles in mesosphere may be affected by the charges attached to them, because image charges will be induced when their distance is close enough along with a strong attractive electric force exerted to them resulting in a collision, this process in polar mesospheric clouds has been initially simulated (Baptiste et al., 2021), it should be emphasized that this image charges-resulted collision is also

https://doi.org/10.5194/egusphere-2022-126
Preprint. Discussion started: 30 May 2022

important in the solar-troposphere link (Zhang and Tinsley, 2017; 2018; Zhang et al., 2018; 2019); another explanation is the ionization of ice particles can help the growth of coagulation and thus enhance the formation of cloud condensation nuclei, it has been studied by simulations and experiments under tropospheric conditions (Svensmark et al., 2017; Yu and Luo, 2014), while it is unknown if it is still valid under the extremely low temperature and low pressure conditions at mesopause. Although the above two explanations provide some insights into the charges-related ice particle formation process in NLCs, the detailed process is still unclear and further investigations are needed.

The mechanism involving the B_y-related changes in the ionosphere-earth current density J_Z in the polar cap produces a change in space charge at the upper and lower boundaries of the NLCs, due to the large reduction of conductivity within NLCs caused by the attachment and recombination of electrons and ions on the ice particles. Gradients of electric field are created as the electric current enters and exits the NLC boundaries, requiring the formation of space charge according to Gauss's Law; this space charge is positive at the cloud top and negative at the cloud base (Zhou and Tinsley, 2007, 2012). Until measurements of electron and ion concentrations and charges on ice crystals become available, it is difficult to evaluate the importance of the B_y-related changes in electric charge and microphysics on the NLCs.

The *IMF* B_y-related mechanisms are concerned more about the microphysical process of ice particle formation and growth, namely, the changes of mean ice particle radius, and are distinct from the *Ly-α* related mechanism, which focuses more on IWC changes. Unlike the *Ly-α* irradiance has a regular 27-day period, the *IMF* B_y varies in a more complex way, thus its effect on NLCs are not necessarily to be regular 27-day periodic. To better understand the effect of solar activity on NLCs at different lags, periods, and latitudes, the *IMF* B_y and *Ly-α* should both be considered in future works.

5 Conclusion

The responses of NLCs to solar wind magnetic fields were investigated using the CIPS/AIM data. Our findings suggest that such a solar-NLC link exists. The mean ice particle radius in NLCs was positively/negatively correlated with the *IMF* B_y in SH/NH on the day-to-day time scale in the majority of NLC seasons during the period of 2007-2017, with a short lag time of 1 day at most. The correlation and sensitivity of r_m versus *IMF* B_y were stronger in the SH, about twice as that in the NH, and more conspicuous in higher latitudes. Similar responses of albedo, IWC and *FO* in NLCs with *IMF* B_y were also noticeable in the SH but not obvious in the NH. The superposed epoch analysis provides further insights into the mean ice particle radius responses during *n2p* and *p2n IMF* B_y reversals in SH and NH, and results show the r_m averagely changes by about 0.73 nm following *IMF* B_y reversals, which is significant at 90% confidence level in the Monte Carlo sensitivity tests. The solar-NLC links are interpreted from the perspective of an *IMF* B_y-driven mechanisms: opposite ionospheric electric potential changes in SH and NH induced by the *IMF* B_y, which change the downward current density J_Z through the NLCs and affects their microphysics. However, it is necessary to further understand the underlying processes of NLCs proposed in above mechanism, and to implement and verify them in polar mesospheric clouds modelling.

https://doi.org/10.5194/egusphere-2022-126
Preprint. Discussion started: 30 May 2022

Data Availability. The version 5.20 CIPS polar mesospheric cloud level 2 data files are available on: http://lasp/colorado/edu/aim/. The solar wind magnetic field data are available on the GSFC/SPDF OMNI Web interface: https://omniweb.gsfc.nasa.gov/form/dx1.html.

Author Contributions. Liang Zhang, Brian Tinsley, and Limin Zhou conceived the idea together. Liang Zhang analyzed the data and drafted the manuscript. Brian Tinsley and Limin Zhou revised the paper and supervised the research.

Competing Interests. The authors declare that they have no conflict of interests.

Acknowledgements. This work was funded by the National Science Foundation of China (No. 41905059) and the Tongji SKL fund (No. 1350231101/055). We are especially grateful to the entire AIM program for providing us the continuous CIPS data, and we further wish to acknowledge the OMNI group for providing high-quality solar wind data.

References

Baptiste, J., Williamson, C., Fox, J., Stace, A. J., Hassan, M., Braun, S., Stamm, B., Mann, I., and Besley, E.: The influence of surface charge on the coalescence of ice and dust particles in the mesosphere and lower thermosphere, Atmospheric Chemistry and Physics, 21, 8735-8745, https://doi.org/10.5194/acp-21-8735-2021, 2021.

Bardeen, C. G., Marsh, D. R., Jackman, C. H., Hervig, M. E., and Randall, C. E.: Impact of the January 2012 solar proton event on polar mesospheric clouds, Journal of Geophysical Research: Atmospheres, 121, 9165–9173, https://doi.org/10.1002/2016JD024820, 2016.

Carstens, J. N., Bailey, S. M., Lumpe, J. D., and Randall, C. E.: Understanding uncertainties in the retrieval of polar mesospheric clouds from the cloud imaging and particle size experiment in the presence of a bright Rayleigh background, Journal of Atmospheric and Solar-Terrestrial Physics, 104, 197–212, https://doi.org/10.1016/j.jastp.2013.08.006, 2013.

Dalin, P., Pertsev, N., Perminov, V., Dubietis, A., Zadorozhny, A., Zalcik, M. et al.: Response of noctilucent cloud brightness to daily solar variations, Journal of Atmospheric and Solar-Terrestrial Physics, 169, 83–90, https://doi.org/10.1016/j.jastp.2018.01.025, 2018.

DeLand, M. T. and Thomas, G. E.: Extending the SBUV PMC data record with OMPS NP, Atmospheric Chemistry and Physics, 19, 7913–7925, https://doi.org/10.5194/acp-19-7913-2019, 2019.

France, J. A., Randall, C. E., Lieberman, R. S., Harvey, V. L., Eckermann, S. D., Siskind, D. E. et al.: Local and remote planetary wave effects on polar mesospheric clouds in the Northern Hemisphere in 2014, Journal of Geophysical Research: Atmospheres, 123, 5149–5162, https://doi.org/10.1029/2017JD028224, 2018.

https://doi.org/10.5194/egusphere-2022-126
Preprint. Discussion started: 30 May 2022

Frederick, J. E. and Tinsley, B. A.: The response of longwave radiation at the South Pole to electrical and magnetic variations: Links to meteorological generators and the solar wind, Journal of Atmospheric and Solar-Terrestrial Physics, 179, 214–224, https://doi.org/10.1016/j.jastp.2018.08.003, 2018.

Frederick, J. E., Tinsley, B. A., and Zhou, L.: Relationships between the solar wind magnetic field and ground-level longwave irradiance at high northern latitudes. Journal of Atmospheric and Solar-Terrestrial Physics, 193, https://doi.org/10.1016/j.jastp.2019.105063, 105063, 2019.

Freeman, M. P., and Lam, M. M.: Regional, seasonal, and inter-annual variations of Antarctic and sub-Antarctic temperature anomalies related to the Mansurov effect. Environmental Research Communications, 1, https://doi.org/10.1088/2515-7620/ab4a84, 111007, 2019.

Gao, H., Li, L., Bu, L., Zhang, Q., Tang, Y., and Wang, Z.: Effect of small-scale gravity waves on polar mesospheric clouds observed from CIPS/AIM, Journal of Geophysical Research: Space Physics, 123, 4026–4045, https://doi.org/10.1029/2017JA024855, 2018.

Hervig, M. E., Siskind, D. E., Bailey, S. M., Merkel, A. W., DeLand, M. T., and Russell, J. M.: The missing solar cycle response of the polar summer mesosphere, Geophysical Research Letters, 46, 10132–10139, https://doi.org/10.1029/2019GL083485, 2019.

Lam, M. M., Chisham, G., and Freeman, M. P.: The interplanetary magnetic field influences mid-latitude surface atmospheric pressure, Environmental Research Letters, 8, https://doi.org/10.1088/1748-9326/8/4/045001, 045001, 2013.

Lam, M. M., Chisham, G., and Freeman, M. P.: Solar wind-driven geopotential height anomalies originate in the Antarctic lower troposphere, Geophysical Research Letters, 41, 6509–6514, https://doi.org/10.1002/2014GL061421, 2014.

Lam, M. M., Freeman, M. P., and Chisham, G.: IMF-driven change to the Antarctic tropospheric temperature due to the global atmospheric electric circuit, Journal of Atmospheric and Solar-Terrestrial Physics, 180, 148–152, https://doi.org/10.1016/j.jastp.2017.08.027, 2018.

Lam, M. M. and Tinsley, B. A.: Solar wind-atmospheric electricity-cloud microphysics connections to weather and climate, Journal of Atmospheric and Solar-Terrestrial Physics, 149, 277–290, https://doi.org/10.1016/j.jastp.2015.10.019, 2016.

Lumpe, J. D., Bailey, S. M., Carstens, J. N., Randall, C. E., Rusch, D. W., Thomas, G. E. et al.: Retrieval of polar mesospheric cloud properties from CIPS: Algorithm description, error analysis and cloud detection sensitivity, Journal of Atmospheric and Solar-Terrestrial Physics, 104, 167–196, https://doi.org/10.1016/j.jastp.2013.06.007, 2013.

Rapp, M. and Thomas, G. E.: Modeling the Microphysics of mesospheric ice particles: Assessment of current capabilities and basic sensitivities, Journal of Atmospheric and Solar-Terrestrial Physics, 68, 715–744, https://doi.org/10.1016/j.jastp.2005.10.015, 2006.

Robert, C. E., von Savigny, C., Rahpoe, N., Bovensmann, H., Burrows, J. P., DeLand, M. T., and Schwartz, M. J.: First evidence of a 27 day solar signature in noctilucent cloud occurrence frequency, Journal of Geophysical Research, 115, 115, D00I12, https://doi.org/10.1029/2009JD012359, 2010.

https://doi.org/10.5194/egusphere-2022-126
Preprint. Discussion started: 30 May 2022

Slyunyaev, N. N., Kalinin, A. V., and Mareev, E. A.: Thunderstorm generators operating as voltage sources in global electric circuit models, Journal of Atmospheric and Solar-Terrestrial Physics, 183, 99–109, https://doi.org/10.1016/j.jastp.2018.12.013, 2019.

Svensmark, H., Enghoff, M. B., Shaviv, N. J., and Svensmark, J.: Increased ionization supports growth of aerosols into cloud condensation nuclei, Nature Communications, 8, 2199, https://doi.org/10.1038/s41467-017-02082-2, 2017.

Thomas, G. E., Thurairajah, B., Hervig, M. E., von Savigny, C., and Snow, M.: Solar-induced 27-day variations of mesospheric temperature and water vapor from the AIM SOFIE experiment: Drivers of polar mesospheric cloud variability, Journal of Atmospheric and Solar-Terrestrial Physics, 134, 56–68, https://doi.org/10.1016/j.jastp.2015.09.015, 2015.

Thurairajah, B., Thomas, G. E., von Savigny, C., Snow, M., Hervig, M. E., Bailey, S. M., and Randall, C. E.: Solar-induced 27-day variations of polar mesospheric clouds from the AIM SOFIE and CIPS experiments, Journal of Atmospheric and Solar-Terrestrial Physics, 162, 122–135, https://doi.org/10.1016/j.jastp.2016.09.008, 2017.

Tinsley, B. A. and Heelis, R. A.: Correlations of atmospheric dynamics with solar activity Evidence for a connection via the solar wind, atmospheric electricity, and cloud microphysics, Journal of Geophysical Research, 98, 10375–10387, https://doi.org/10.1029/93JD00627, 1993.

Tinsley, B. A., Zhou, L., Wang, L., and Zhang, L.: Seasonal and solar wind sector duration influences on the correlation of high latitude clouds with ionospheric potential, Journal of Geophysical Research: Atmospheres, 126, https://doi.org/10.1029/2020JD034201, 2021.

Williams, E. and Mareev, E.: Recent progress on the global electrical circuit, Atmospheric Research, 135–136, 208–227, https://doi.org/10.1016/j.atmosres.2013.05.015, 2014.

Winkler, H., von Savigny, C. V., Burrows, J. P., Wissing, J. M., Schwartz, M. J., Lambert, A., and García-Comas, M: Impacts of the January 2005 solar particle event on noctilucent clouds and water at the polar summer mesopause, Atmospheric Chemistry and Physics, 12, 5633–5646, https://doi.org/10.5194/acp-12-5633-2012, 2012.

Yu, F. and Luo, G.: Effect of solar variations on particle formation and cloud condensation nuclei, Environmental Research Letters, 9, 045004, https://doi.org/10.1002/2016JD026255, 2014.

Zhang, L. and Tinsley, B. A.: Parameterization of aerosol scavenging due to atmospheric ionization under varying relative humidity, Journal of Geophysical Research: Atmospheres, 122, 5330–5350, https://doi.org/10.1002/2016JD026255, 2017.

Zhang, L. and Tinsley, B. A.: Parameterization of in-cloud aerosol scavenging due to atmospheric ionization: 2. Effects of varying particle density, Journal of Geophysical Research: Atmospheres, 123, 3099–3115, https://doi.org/10.1002/2017JD027884, 2018.

Zhang, L., Tinsley, B. A., and Zhou, L.: Parameterization of in-cloud aerosol scavenging due to atmospheric ionization: part 3. Effects of varying droplet radius, Journal of Geophysical Research: Atmospheres, 123, 10–546, https://doi.org/10.1029/2018JD028840, 2018.

https://doi.org/10.5194/egusphere-2022-126
Preprint. Discussion started: 30 May 2022

Zhang, L., Tinsley, B., and Zhou, L.: Parameterization of in-cloud aerosol scavenging due to atmospheric ionization: part 4. Effects of varying altitude, Journal of Geophysical Research: Atmospheres, 124, 13105–13126, https://doi.org/10.1029/2018JD030126, 2019.

Zhou, L. and Tinsley, B. A.: Production of space charge at the boundaries of layer clouds, Journal of Geophysical Research, 112, D11203, https://doi.org/10.1029/2006JD007998, 2007.

Zhou, L. and Tinsley, B. A.: Time dependent charging of layer clouds in the global electric circuit, Advances in Space Research, 50, 828–842, https://doi.org/10.1016/j.asr.2011.12.018, 2012.

https://doi.org/10.5194/egusphere-2022-126
Preprint. Discussion started: 30 May 2022

Table 1. Dates (year - day of year) of *p2n* and *n2p IMF* B_y reversals during 2007 and 2017 in NH and SH summer.

***p2n*, NH summer**			
2007-159	2007-172	2007-184	2007-199
2007-227	2008-159	2008-186	2008-212
2009-171	2009-203	2010-176	2011-172
2011-198	2012-170	2012-181	2012-211
2012-225	2013-166	2013-220	2014-168
2014-184	2014-195	2014-208	2014-222
2015-158	2015-184	2015-211	2016-174
2016-201			
***n2p*, NH summer**			
2007-164	2007-180	2007-192	2007-218
2008-177	2009-160	2009-194	2009-223
2010-158	2010-189	2010-220	2011-163
2011-190	2011-219	2012-163	2012-175
2012-204	2012-221	2013-180	2014-160
2014-176	2014-188	2014-212	2015-163
2015-192	2015-218	2016-162	2016-188
***n2p*, SH summer**			
2007-351	2008-12	2008-353	2008-364
2009-23	2009-355	2010-17	2010-357
2011-16	2012-25	2012-40	2012-343
2013-2	2013-11	2013-36	2013-355
2014-19	2014-346	2015-6	2015-36
2015-362	2016-17	2016-26	
***p2n*, SH summer**			
2008-31	2008-357	2009-8	2010-5
2010-30	2011-6	2011-25	2012-6
2012-33	2012-359	2013-6	2014-11
2014-39	2014-356	2015-20	2016-11
2016-20	2016-38		

330

https://doi.org/10.5194/egusphere-2022-126
Preprint. Discussion started: 30 May 2022

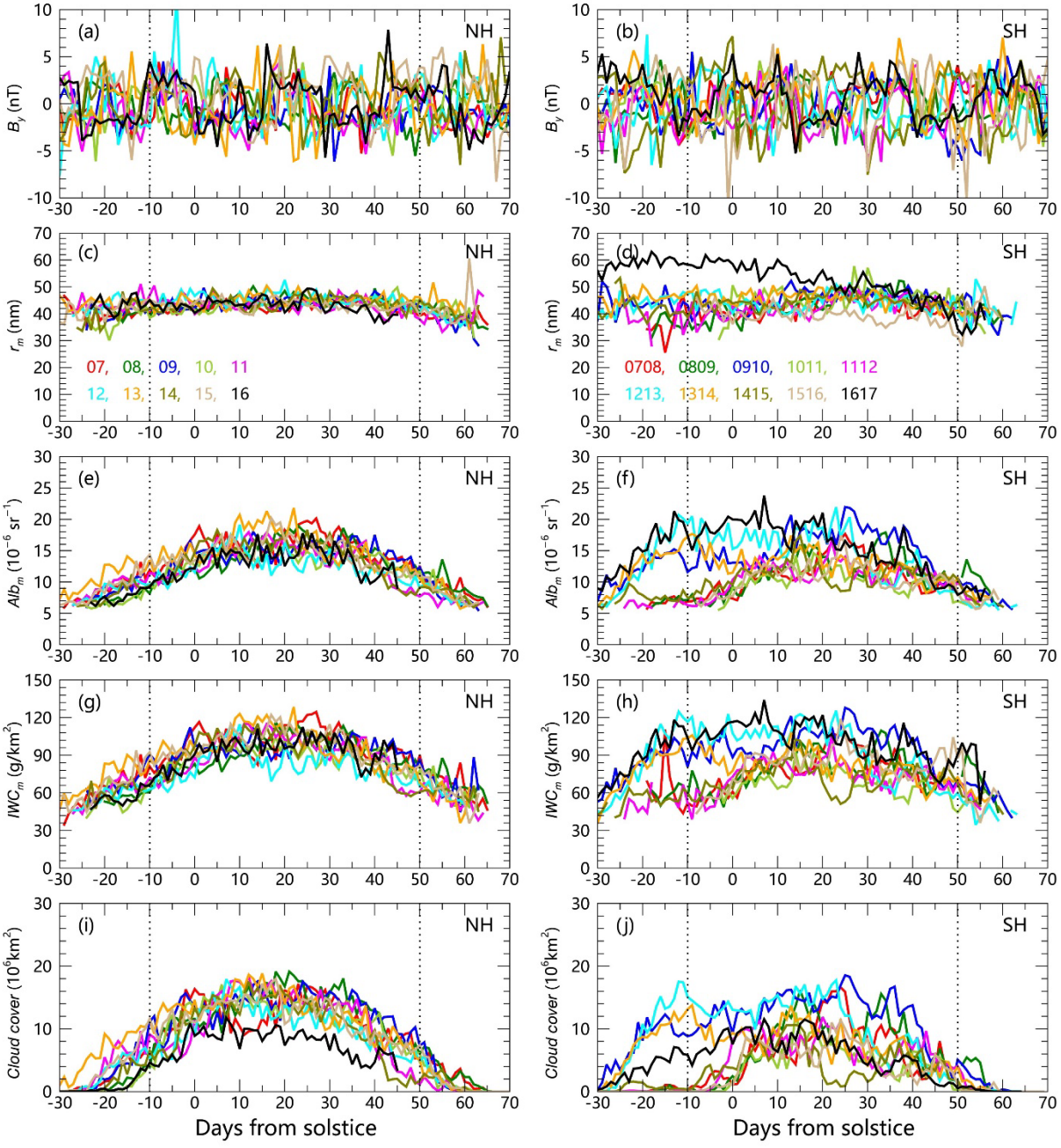

Figure 1. Daily-averaged *IMF* B_y, mean ice particle radius (r_m), mean albedo (Alb_m), mean ice water content (IWC_m), and cloud cover observed by CIPS for NH (left) and SH (right) for each of the NLC seasons from 2007 through 2017.

https://doi.org/10.5194/egusphere-2022-126
Preprint. Discussion started: 30 May 2022

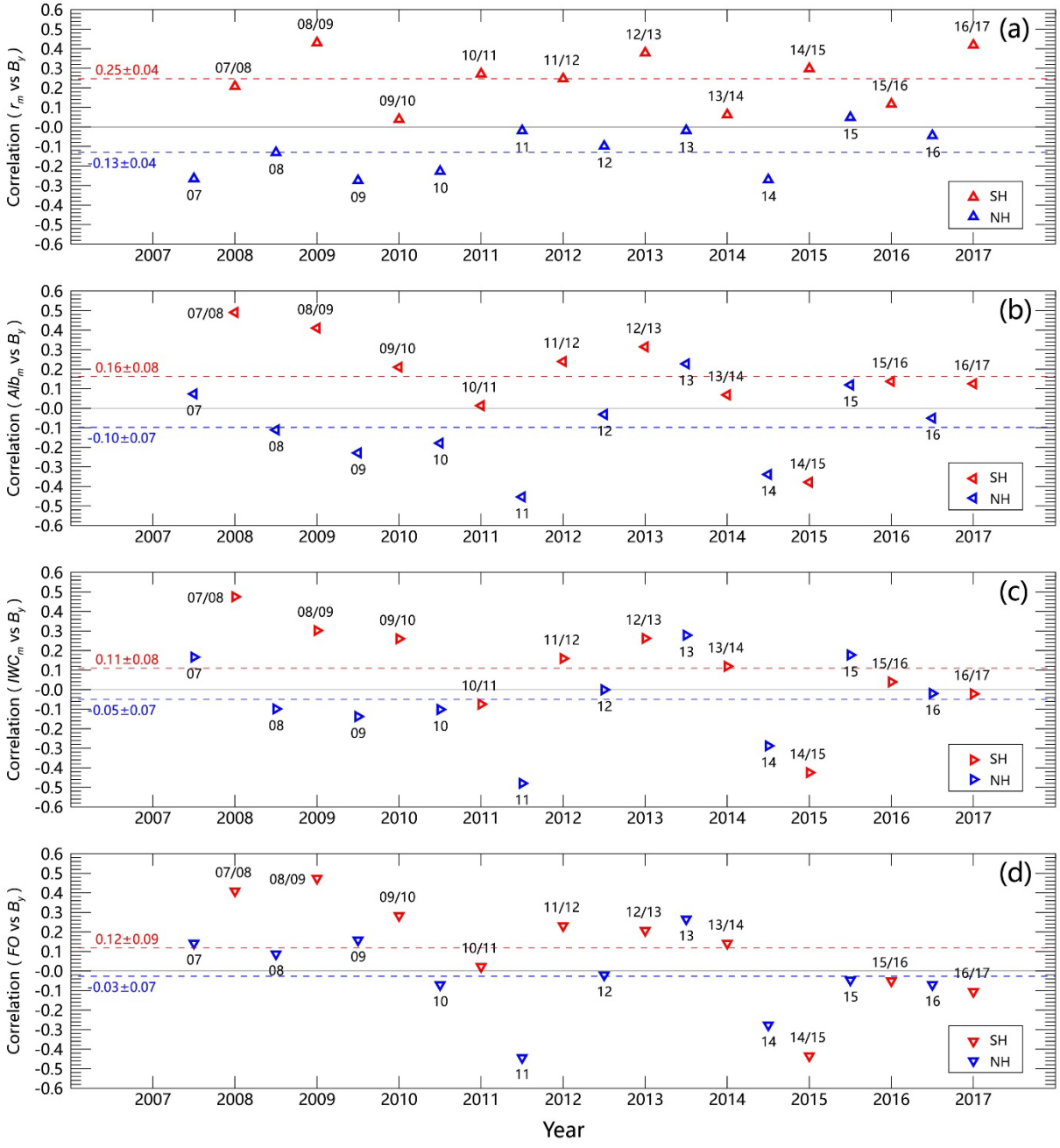

335

Figure 2. Correlation coefficients between the anomaly of r_m, Alb_m, IWC_m and $IMF\ B_y$ from 2007 to 2017, with red/blue symbols representing the seasonal correlation coefficients and dashed red/blue lines illustrating the mean correlation coefficients for the SH and NH, respectively.

https://doi.org/10.5194/egusphere-2022-126
Preprint. Discussion started: 30 May 2022

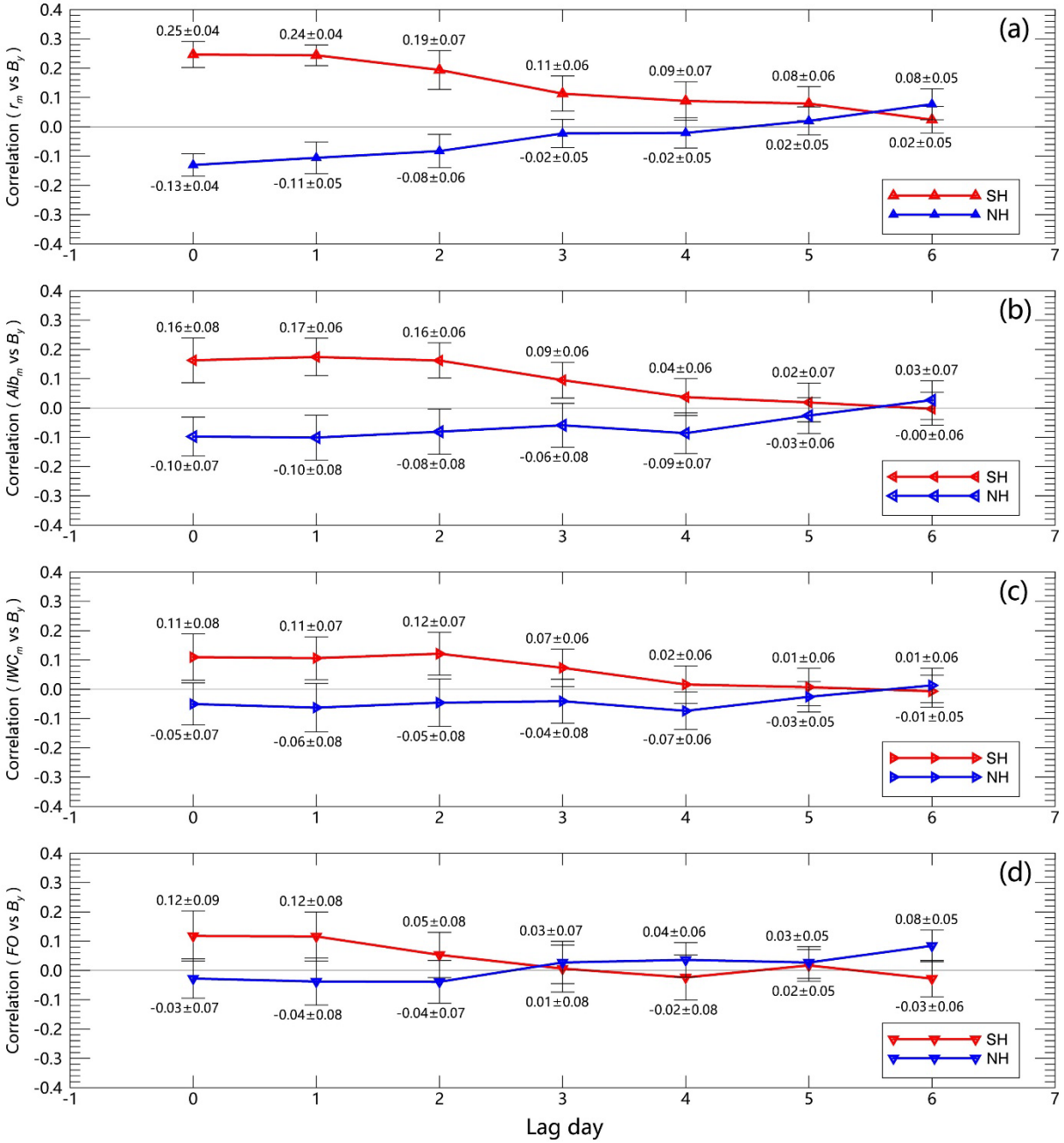

Figure 3. Correlation coefficients between the anomaly of r_m, Alb_m, IWC_m and $IMF\ B_y$ for time lags varying from 0 to 6 days, with red/blue lines representing the mean correlation coefficients and error bars illustrating the standard deviation of the mean for the SH and NH respectively.

https://doi.org/10.5194/egusphere-2022-126
Preprint. Discussion started: 30 May 2022

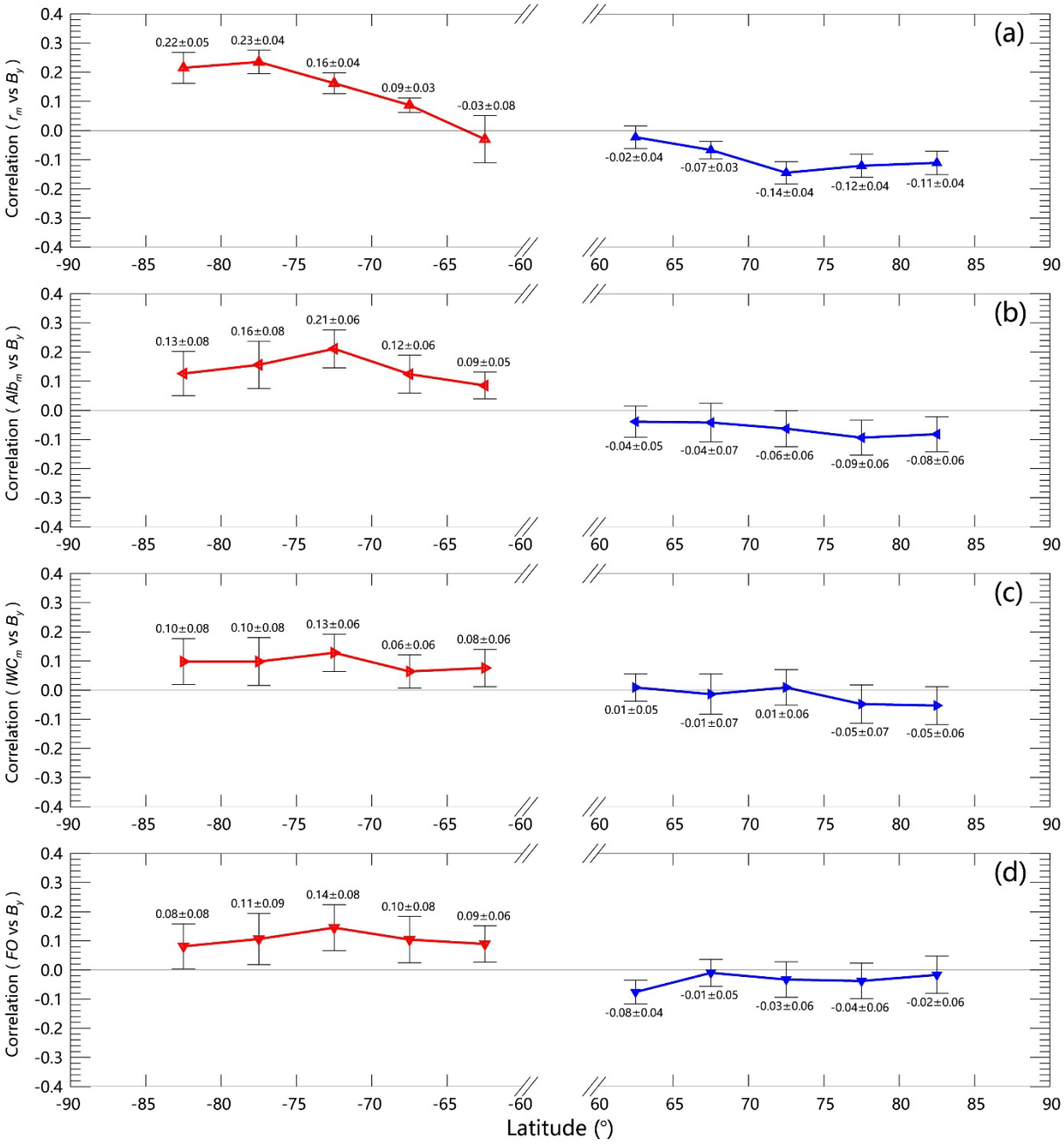

Figure 4. Correlation coefficients between the anomaly of r_m, Alb_m, IWC_m and *IMF* B_y at different latitude bands, with red/blue lines representing the mean correlation coefficients and error bars illustrating the standard deviation of the mean for the SH and NH respectively.

https://doi.org/10.5194/egusphere-2022-126
Preprint. Discussion started: 30 May 2022

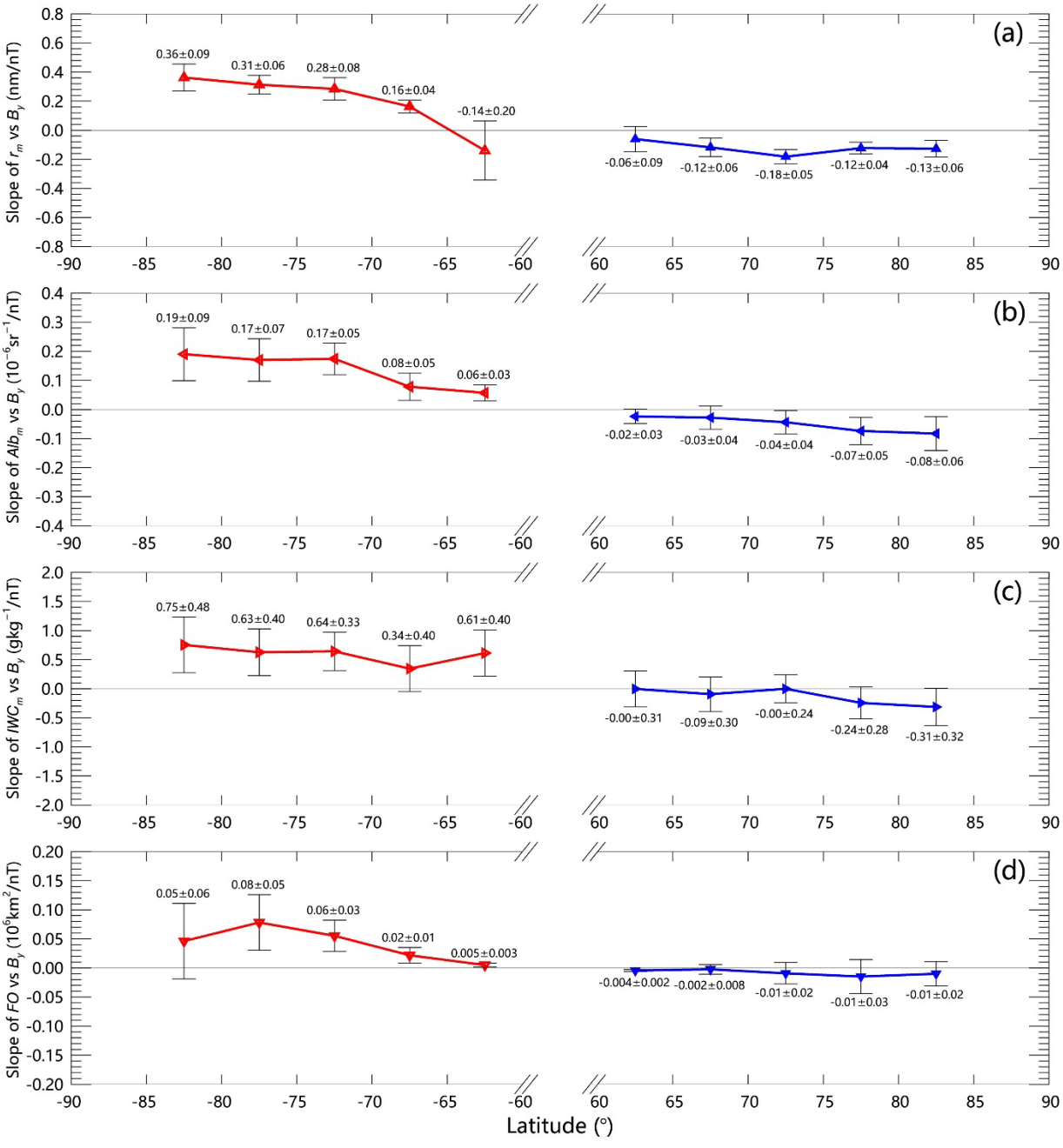

Figure 5. Slope of the anomaly of r_m, Alb_m, IWC_m versus $IMF\ B_y$ at different latitude bands, with red/blue lines representing the mean slope and error bars illustrating the standard deviation of the mean for the SH and NH respectively.

https://doi.org/10.5194/egusphere-2022-126
Preprint. Discussion started: 30 May 2022

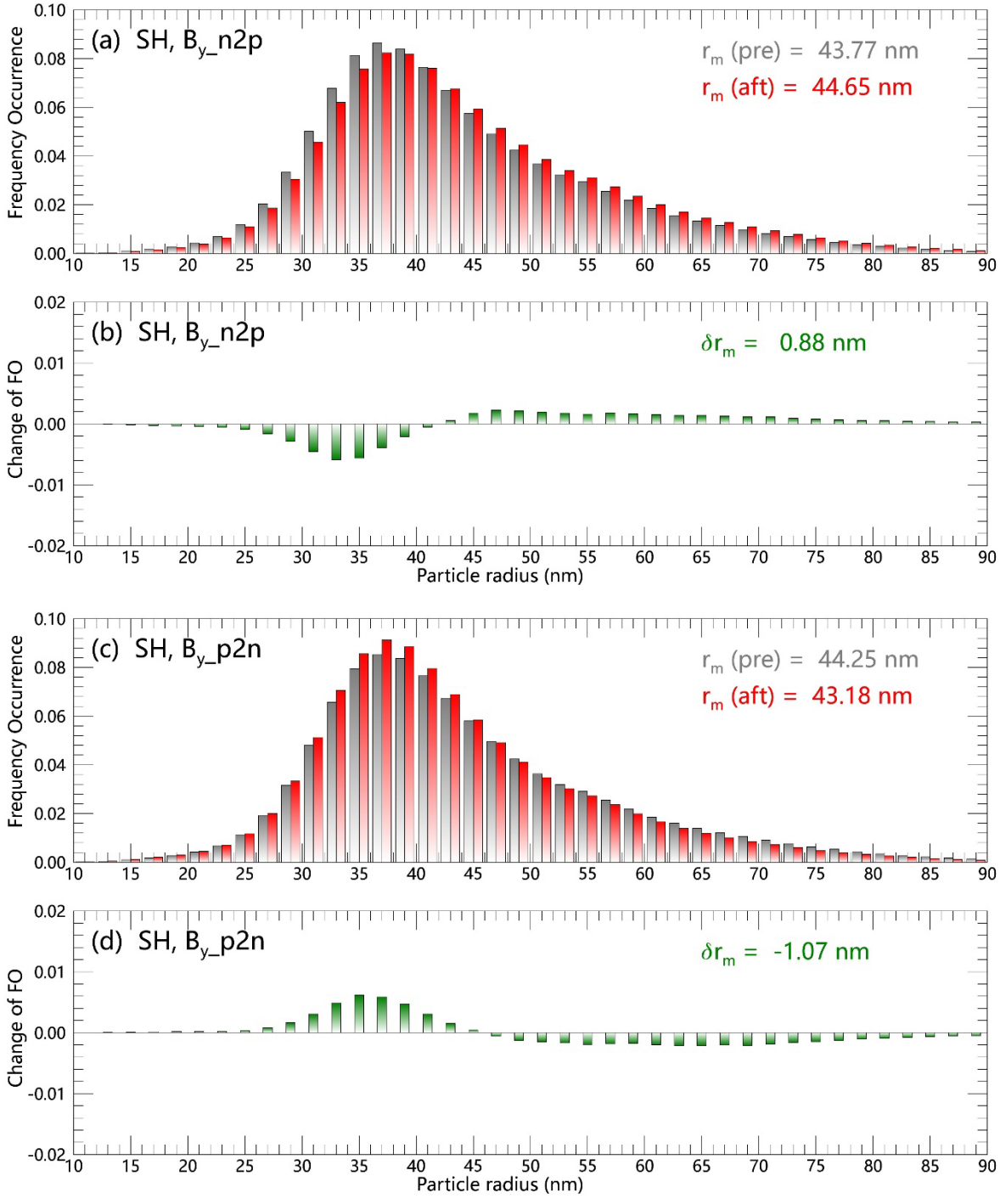

Figure 6. Changes of ice particle radius distribution $\delta f(r)$ during *n2p* and *p2n IMF* B_y reversals in the southern hemisphere. The distributions of r over all pixels on three days before/after the key days are indicated by the gray/red bars, and the changes between them are shown by the green bars.

https://doi.org/10.5194/egusphere-2022-126
Preprint. Discussion started: 30 May 2022

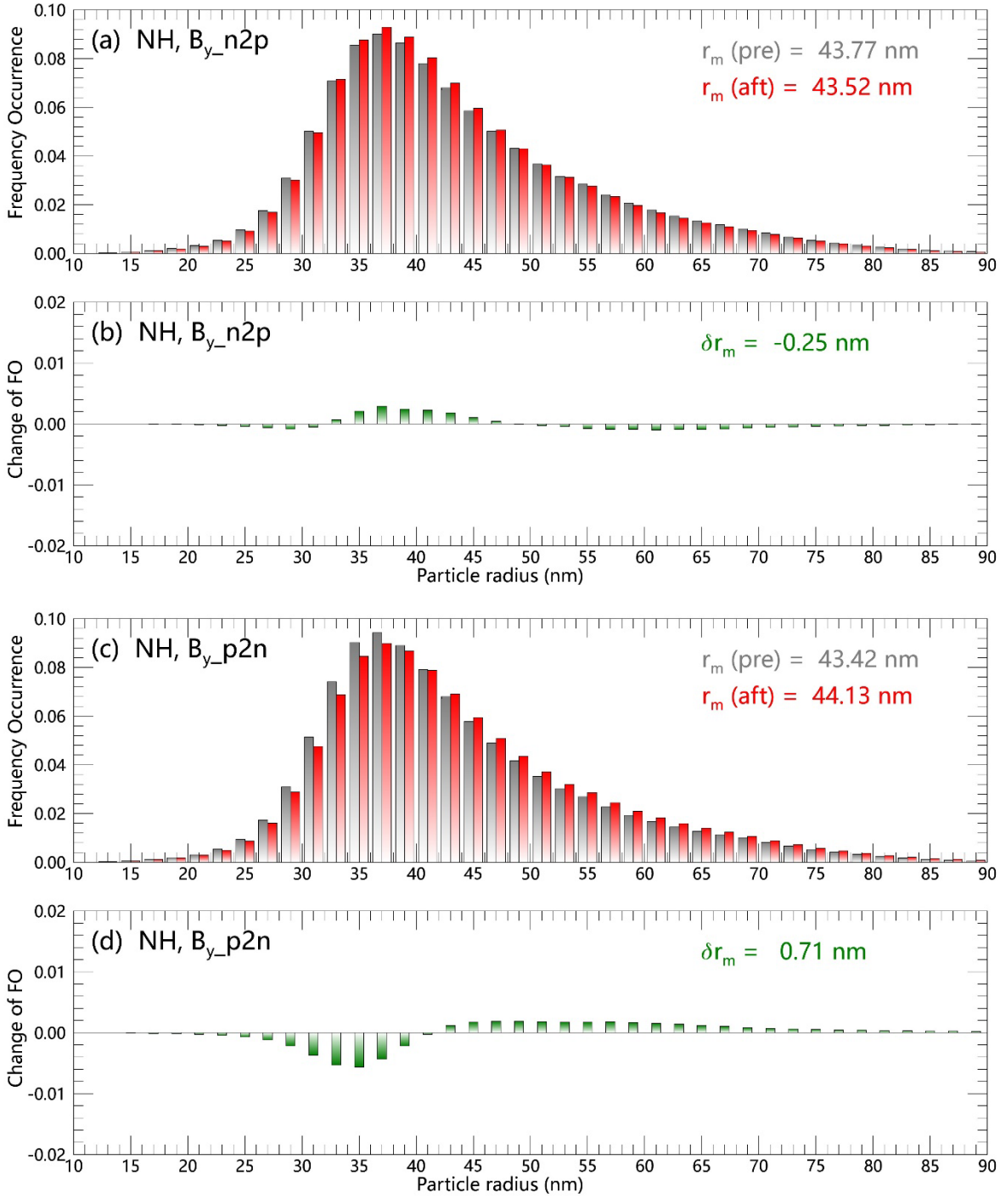

Figure 7. Similar as Figure 6, but for the results of the northern hemisphere.

https://doi.org/10.5194/egusphere-2022-126
Preprint. Discussion started: 30 May 2022

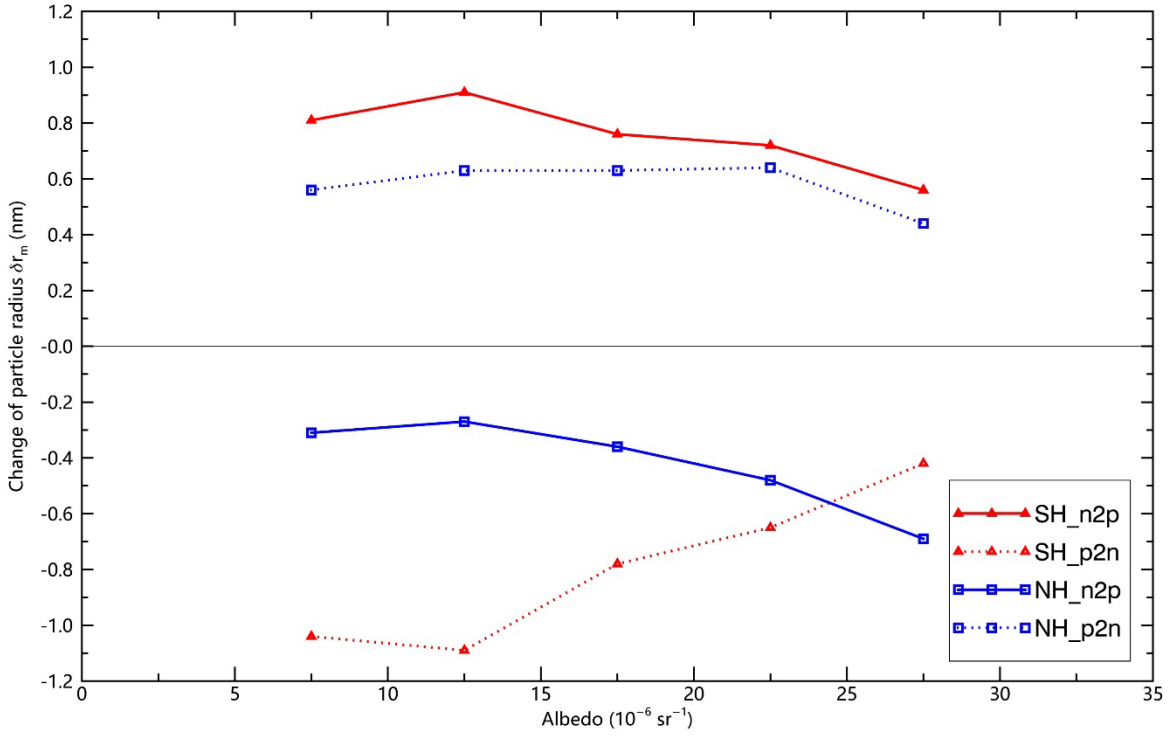

Figure 8. The influences of *IMF* B_y reversals on the ice particle radius changes δr_m at different NLCs brightness.